Second-order electromagnetic transitions of nuclei

Author: Daniel Castillo Garcia
Facultat de Física, Universitat de Barcelona, Diagonal 645, 08028 Barcelona, Spain.

Advisor: Javier Menéndez

Abstract: The excited states of atomic nuclei typically decay via electromagnetic transitions. In this work, we study second-order electromagnetic double-magnetic dipole transitions for different nuclei: ^{20}Ne, ^{48}Ti, ^{40}Ca and ^{72}Ge. We calculate nuclear matrix elements using the nuclear shell model with different valence spaces and nuclear interactions, and we estimate the quality of the results by comparing related calculations with data of first-order electromagnetic transitions and energy spectra. The theoretical results can be used to predict second-order electromagnetic half-lives which could be compared with future experiments.

I. INTRODUCTION

Double-gamma transitions are second-order electromagnetic (EM) processes in which two photons (γ) are simultaneously emitted, leaving atomic nuclei in a lower energy state. This decay occurs through virtual intermediate states, such as excited nuclear states or interactions with other particles, unlike first-order decays, which occur directly between initial and final states. These processes have been a subject of extensive study during the past two decades, as they can provide new information about nuclear structure, such as generalized nuclear electric polarizabilities and magnetic susceptibilities [1]. However, the observation of these decays is challenging, because these transitions are natural competitors of first-order electromagnetic decays, which are much more probable. Therefore, until relatively recently, second-order EM decays could only be observed in nuclei where their first excited state has the same spin-parity as the ground state ($0^+_2 \to 0^+_{GS}$). For these transitions, single-gamma decays are forbidden. It was not until 2015 [2] that double-gamma decays competing against first-order transitions could be observed. In particular, for ^{137}Ba, the transition from the state $J^\pi = 11/2^-$ to the ground state $J^\pi = 3/2^+$ was successfully measured.

Furthermore, a good correlation has been found between double-beta neutrinoless transitions ($0\nu\beta\beta$) and EM double-magnetic dipole decays ($M1M1$). The linear correlation has been observed for shell model calculations when the two photons share the energy of the decay [1]. This is very interesting because understanding $0\nu\beta\beta$ decay could provide information about the unknown absolute mass of neutrinos and could offer insights regarding the dominance of matter in our universe.

The main objective of this work is the study of $\gamma\gamma$ transitions for different nuclei. We study ^{20}Ne and ^{48}Ti nuclei because these calculations are easier to control. On the other hand, there is experimental interest in measuring $M1M1$ transitions for the other nuclei studied, ^{40}Ca and ^{72}Ge. This work is a first step to quantify the probability of second-order $M1M1$ ($0^+ \to 0^+$) decays. In order to do so, we calculate $M1M1$ nuclear matrix elements (NMEs) in the framework of nuclear shell model.

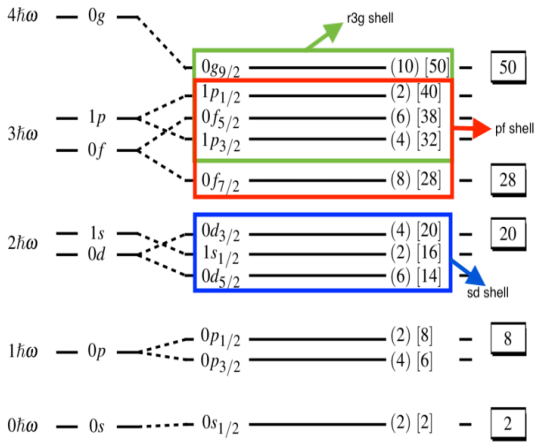

FIG. 1: Nuclear shell model single-particle orbitals adapted from [3]. The blue box indicates the sd shell, the red box the pf shell and the green box the r_3g valence space.

II. NUCLEAR SHELL MODEL

The nuclear shell model uses the Pauli exclusion principle to describe atomic nuclei in terms of single-particle levels. The origin of this framework came from the prediction of magic numbers (2, 8, 20, 28, 50, 82, 126) for which protons or neutrons tend to have stronger binding energies and are more resistant to nuclear decays. A nuclear mean field can describe these magic numbers [4],

$$U(r) = \frac{1}{2} m_N \omega^2 r^2 + D\vec{l}\cdot\vec{l} - C\vec{l}\cdot\vec{s}, \qquad (1)$$

with three contributions: the harmonic oscillator term, which depends on the nucleon mass (m_N), the frequency (ω) and the position ($\vec{r}$); the orbital angular momentum ($\vec{l}$) interaction; and the third term, the spin-orbit ($\vec{s}$ represents the spin) interaction. D and C are constants. In this mean-field approximation, wavefunctions are Slater

determinants,

$$|\phi_\alpha\rangle = \prod_{i=nlmj\tau} a_i^\dagger |0\rangle, \tag{2}$$

where n, l, m, j and τ are the quantum numbers describing the single particle state i. n indicates the radial quantum number, l is the orbital angular momentum, j corresponds to the total angular momentum, m is the j projection, and τ is the isospin. $a_i^\dagger$ is an operator that creates a particle in the i state and $|0\rangle$ is the vacuum state [5]. However, to achieve a better description of the nucleus, it is necessary to add an effective interaction between nucleons. This leads to the interacting nuclear shell model, which is characterized by an effective Hamiltonian (H_{eff}) that consists of one-body operators, including kinetic energy and mean field potential, as well as a two-body operators representing the interaction between neutrons and protons. Now, the wavefunctions are linear combinations of Slater determinants,

$$|\Phi\rangle = \sum_\alpha C_\alpha |\phi_\alpha\rangle. \tag{3}$$

In order to reduce the complexity of the many-body problem, the configuration space is divided in three parts:

- Inert core: Orbitals which are always full of nucleons.
- Valence space: Orbitals available for the valence nucleons, partially occupied. These orbitals are involved in the effective interaction.
- External space: Empty orbitals.

The dimension of the valence space (Slater determinants within this space) is the product of the combinatorial numbers given by the degeneracy of the space and the number of valence nucleons [4],

$$dim_{vs} = \binom{n_s}{n_v} \cdot \binom{z_s}{z_v}. \tag{4}$$

Here, n_s and z_s represent the available single-particle states in the valence space, while n_v and z_v denote the nucleon number within this space, with n index for neutrons and z for protons. In this study, we use ANTOINE, a nuclear shell model code capable of handling 10^9 Slater determinants [6]. Table I indicates the number of Slater determinants of all the calculations presented in this work.

III. M1M1 NUCLEAR MATRIX ELEMENT

Our main goal is to obtain $M1M1$ NMEs. This transition is governed by the $M1$ operator,

$$M1 = \mu_n \sqrt{\frac{3}{4\pi}} \sum_{i=1}^{A} (g_i^l \vec{l}_i + g_i^s \vec{s}_i), \tag{5}$$

Nucleus	Valence space	Slater determinants
^{20}Ne	sd shell	$4 \cdot 10^2$
^{48}Ti	pf shell	$4 \cdot 10^5$
^{40}Ca (tr.1)	$sdpf$ shell; without $p_{1/2}$	$4 \cdot 10^8$
^{40}Ca (tr.2)	$sdpf$ shell; pf truncated	$5 \cdot 10^8$
^{40}Ca (tr.3)	$sdpf$ shell; $0f_{5/2}$, $1p_{3/2}$, $1p_{1/2}$ truncated	$1 \cdot 10^9$
^{72}Ge	r_3g	$7 \cdot 10^7$

TABLE I: Valence spaces and number of Slater determinants for the shell-model calculations of the nuclei studied in this work.

where μ_n is the nuclear magneton and $g_n^l = 0$, $g_p^l = 1$, $g_n^s = -3.826$ and $g_p^s = 5.586$ are the orbital and spin g-factors [7], for neutrons (n) and protons (p). The sum is over all A nucleons in the nucleus.

For $M1M1$ transitions, the nuclear matrix element is,

$$\mathcal{M}^{\gamma\gamma} = \sum_n \frac{\langle 0_f^+ || M1 || 1_n^+ \rangle \langle 1_n^+ || M1 || 0_i^+ \rangle}{\epsilon_n (1 - \frac{\Delta\epsilon^2}{2\epsilon_n^2})}, \tag{6}$$

with $\Delta\epsilon = k_0 - k_0'$, k_0 and k_0' the photon energies and $\epsilon_n = E_n - \frac{E_i + E_f}{2}$. E_i, E_f and E_n correspond to the energy of the initial, final and intermediate states, respectively. To avoid the dependence on the photon energies, we demand that they share the transition energy: $k_0 = k_0' = Q_{EM}/2$, where $Q_{EM} = E_f - E_i$, and in consequence $\Delta\epsilon = 0$ [1]. In the numerator, the double bars indicate reduced matrix elements, following the Wigner-Eckart theorem [5]. Considering all this, we calculate,

$$\mathcal{M}^{\gamma\gamma}(M1M1) = \sum_n \frac{\langle 0_f^+ || M1 || 1_n^+ \rangle \langle 1_n^+ || M1 || 0_i^+ \rangle}{\epsilon_n}. \tag{7}$$

In order to evaluate the previous expression we use the following procedure:

1. We determine $|0_{GS}^+\rangle$ (final state, $|0_f^+\rangle$) and $|0_i^+\rangle$ (initial state) by solving the Schrödinger equation,

$$H_{eff}|0_{GS}^+\rangle = E_{GS}|0_{GS}^+\rangle,\ H_{eff}|0_1^+\rangle = E_1|0_1^+\rangle, \tag{8}$$

   for the effective Hamiltonian, H_{eff}.

2. We apply the $M1$ operator to $|0_{GS}^+\rangle$ and $|0_i^+\rangle$, obtaining $M1|0^+\rangle$ for both states.

3. It is not viable to calculate directly the huge amount of 1^+ states. Hence we apply the Lanczos' strength function method [4] to expand,

$$M1|0_i^+\rangle = \sum_n a_n |1_n^+\rangle, \tag{9}$$

   where n is a finite number determined by the number of iterations we choose. The different 1^+ approximate eigenstates have energies, E_n, and overlaps, a_n, with the $M1|0_i^+\rangle$ state.

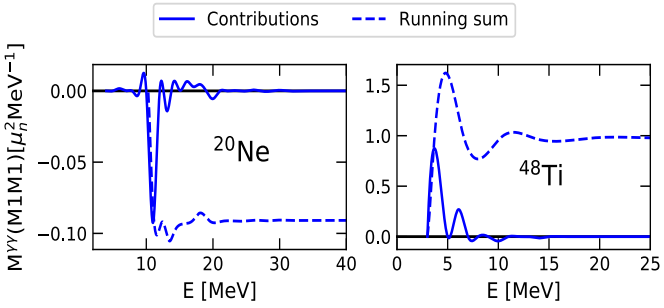

FIG. 2: Running sum of the $M1M1$ matrix elements for ^{48}Ti (right) and ^{20}Ne (left) as a function of the energy of the intermediate states.

4. Finally, we calculate the overlap of the $|1_n^+\rangle$ states with $M1|0_{GS}^+\rangle$ ($\langle 0_{GS}^+||M1||1_n^+\rangle$). We now have all the necessary elements to calculate the $M1M1$ NME in Eq.(7).

At this point, it is important to emphasize that since the 1_n^+ states obtained are approximate and therefore not exact eigenstates of the Hamiltonian, it is necessary to verify the convergence of the result. Taking into account Eq.(7), for the numerator, the completeness relation gives the exact result,

$$\sum_n \langle 0_{GS}^+|M1|1_n^+\rangle\langle 1_n^+|M1|0_i^+\rangle = \langle 0_{GS}^+||M1M1||0_i^+\rangle, \tag{10}$$

where index n runs for all eigenstates 1_n^+ of H_{eff}. We have found that for 10 iterations with the Lanczos' method the results converge for all the nuclei studied.

IV. RESULTS

A. ^{20}Ne and ^{48}Ti

We perform shell model calculations with a ^{16}O core for ^{20}Ne and a ^{40}Ca core for ^{48}Ti. Therefore, we have 2 neutrons and 2 protons in the sd-shell for ^{20}Ne, calculated with the USDB [7] interaction to describe the $M1M1(0_5^+ \to 0_{GS}^+)$ transition. For ^{48}Ti we have 6 neutrons and 2 protons in the pf-shell, calculated with the KB3G interaction [4] to describe the $M1M1(0_2^+ \to 0_{GS}^+)$ transition. We obtain, $\mathcal{M}^{\gamma\gamma}(M1M1) = -0.091\ \mu_n^2$ MeV^{-1} for ^{20}Ne and $\mathcal{M}^{\gamma\gamma}(M1M1) = -0.97\ \mu_n^2$ MeV^{-1} for ^{48}Ti.

Figure 2 shows that, in the case of ^{20}Ne, the negative contributions from the first excited levels are dominant. This can be explained by two reasons: Firstly, the contributions of the numerator for higher-lying 1^+ levels are small. Additionally, since we study the transition from the fifth excited 0_5^+ state to the ground state, the significant energy difference between the final and initial states reduces the contribution of excited states that are not close to the ground state. On the other hand, Figure 2 also shows that, for ^{48}Ti, the first peak dominates. Even though the contributions to the numerator from the first and second 1^+ states are similar, since 1_2^+ is excited by 3 MeV with respect to 1_1^+, the contribution to the $M1M1$ NME of 1_2^+ is reduced by a factor of four compared to 1_1^+ due to the energy denominator in Eq.(7).

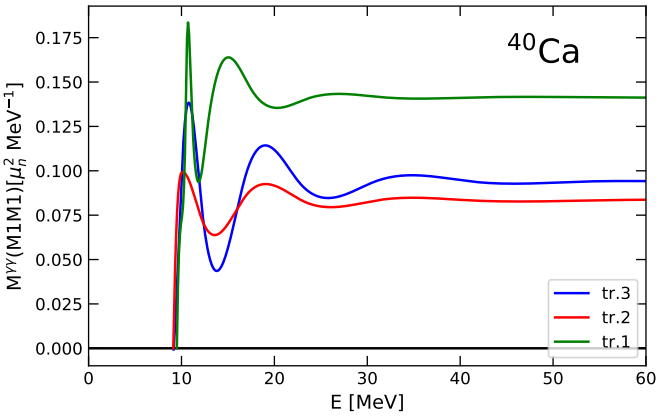

FIG. 3: $M1M1$ matrix element running sum for the different truncated valence spaces used for ^{40}Ca.

B. ^{40}Ca

For the calculation of ^{40}Ca we use a ^{16}O core. We have used the sdpf.ca40.prc interaction [4] working on the sd- and pf-shells with 12 neutrons and 12 protons, and the $0d_{5/2}$ orbital fully occupied. We study the decay from the second excited level (0_2^+) to the ground state (0_{GS}^+). However, in this case, the dimension of the full valence space is too large, 10^{12} Slater determinants. Therefore, we reduced it by either removing the $1p_{1/2}$ orbital (tr.1) or truncating certain orbitals (tr.2 and tr.3), allowing for a maximum of 6 nucleons in them. This limits the occupancy for the specific orbitals listed in Table I. In other words, we do not allow Slater determinants in Eq.(3) with more than 6 nucleons combined in the truncated orbitals.

Figure 3 shows that the NME behaviour is very similar

	$\mathcal{M}^{\gamma\gamma}(M1M1)[\mu_n^2 \text{MeV}^{-1}]$	Q_{EM} [MeV]
^{40}Ca (tr.1)	0.14	5.25
^{40}Ca(tr.2)	0.083	3.49
^{40}Ca (tr.3)	0.094	3.91
EXP.		3.35 [8]

TABLE II: $M1M1$ matrix elements and energy difference between final and initial state for ^{40}Ca. Theoretical results compared to experiment.

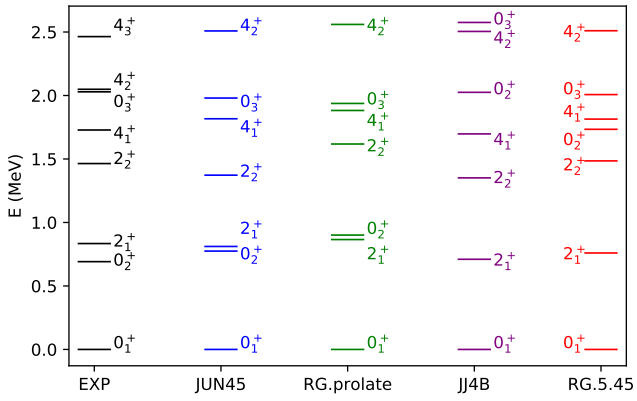

FIG. 4: Calculated ^{72}Ge low-lying spectra for the four shell-model interactions, compared to the experimental data [8]. The states are labelled by the total angular momentum and parity, J^P.

for all three cases. The NME value is predominantly determined by the first four excited 1^+ levels. For tr.1, the contributions in the numerator are larger, leading to a bigger NME. The other truncations, tr.2 and tr.3, give similar results, but the M1M1 NME is larger for tr.3. Table II indicates that tr.2 is the one with Q_{EM} closest to the experimental value. This favors the result obtained with tr.2, which we consider the most reliable.

C. ^{72}Ge

Finally, for ^{72}Ge we perform shell model calculations with a ^{56}Ni core, in a valence space with 12 neutrons and 4 protons distributed in the r_3g valence space, see Figure 1.We have considered four interactions, JUN45, RG.prolate, JJ4B, and RG.5.45 [1].

In order to obtain an initial perspective on which interactions could provide a better description for this nucleus, we compute the seven lowest-energy states of ^{72}Ge with these four interactions. Figure 4 shows that, in general, the second excited states for different angular momentum (J) values are not correctly described by any of them. Moreover, JJ4B and RG.5.45 deviate the most from the experimental data, as the 0_2^+ state does not reproduce the measured excitation energy. The other two interactions represent the energy of the initial and final states involved in the studied transition ($0_2^+ \to 0_{GS}^+$) much better, see Table IV.

In addition, we calculate EM $E2$ and $M1$ reduced transition probabilities to verify if JUN45 and RG.prolate describe well this nucleus. The $E2$ operator is defined as,

$$E2 = \sum_{i=1}^{A} e_i r_i^2 Y_{20}(\theta_i, \phi_i) \tag{11}$$

	EXP.	JUN45	RG.prolate	JJ4B	RG.5.45
$\delta(E2/M1)$	-10.30	-0.14	-0.27	-0.39	-0.23
Q_{quad} [e·fm^2]	-13.00	12.85	10.98	16.79	17.79
μ [μ_n]	0.77	0.54	0.45	0.46	0.57

TABLE III: Mixing ratio for the $2_2^+ \to 2_1^+$ transition and quadrupole, magnetic moment for the $J = 2_1^+$ state, for the four interactions used for ^{72}Ge. Theoretical results are compared to experiment [8].

	$\mathcal{M}^{\gamma\gamma}(M1M1)[\mu_n^2\text{MeV}^{-1}]$	Q_{EM} [MeV]
^{72}Ge (JUN45)	0.011	0.77
^{72}Ge (RG.prolate)	-0.043	0.90
^{72}Ge (JJ4B)	0.29	2.03
^{72}Ge (RG.5.45)	0.18	1.73
EXP.		0.69 [8]

TABLE IV: $M1M1$ matrix elements and energy difference between final and initial state for ^{72}Ge. Theoretical results are compared to experiment.

where e is the electric charge, Y_{20} is the spherical harmonic and r, θ and ϕ correspond to spherical coordinates. We compare the mixing ratio of the $2_2^+ \to 2_1^+$ transition with experimental data. The mixing ratio compares $E2$ with $M1$ transitions as follows,

$$\delta(E2/M1) = 83.5 Q_{EM} \Delta(E2/M1) \frac{\mu_n}{e\text{fm}^2\text{MeV}}, \tag{12}$$

where $\Delta(E2/M1) = \frac{(2_2^+||E2||2_1^+)}{(2_2^+||M1||2_1^+)}$ [5]. Table III indicates that, for all the interactions, the $M1$ transition exhibits a greater strength compared to experiment and the $E2$ strength.

We also calculate the quadrupole moments and magnetic moments [5],

$$\begin{aligned} Q_{quad} &= \sqrt{\frac{16\pi}{5}} \sqrt{\frac{J(2J-1)}{(J+1)(2J+1)(2J+3)}} (2_1^+||E2||2_1^+), \\ \mu &= \sqrt{\frac{4\pi}{3}} \sqrt{\frac{J}{(J+1)(2J+1)}} (2_1^+||M1||2_1^+), \end{aligned} \tag{13}$$

as they have a strong correlation with the reduced transition probabilities $E2$ [9] and $M1$. The results in Table III show that, for JUN45 and RG.prolate, the absolute values of Q_{quad} are near to the experimental one, but they have the opposite sign. The μ values are smaller than μ_{EXP} for all the interactions. Hence, important differences compared to experimental data appear.

As none of the four interactions provides a fully satisfactory description of the nucleus, we calculate the $M1M1$ matrix elements for all of them. Figure 5 shows that, for JUN45, there are significant contributions from the first excited levels, but they mostly cancel each other.

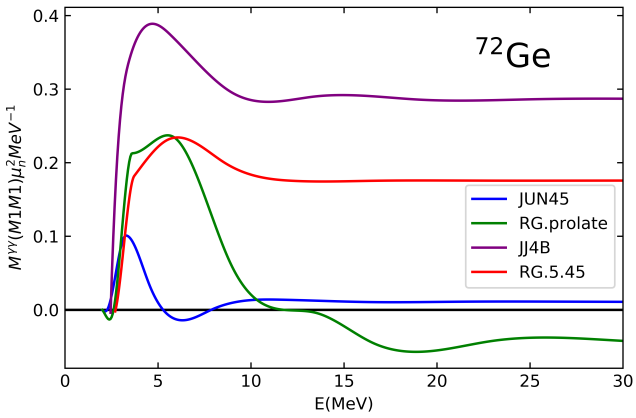

FIG. 5: Running sum of the $M1M1$ matrix element for the four interactions used for the ^{72}Ge nucleus.

Specifically, the contribution of the 1_1^+ state cancels with the ones of 1_2^+ and 1_3^+. On the other hand, in the case of RG.prolate, we find large contributions in the numerator for relatively high-energy excited states, even extending to a significant one from the 1_5^+ state. There is a substantial cancellation as the 1_1^+ state, favoured by the energy denominator, has the opposite sign compared to all other notable contributions. Finally, for the JJ4B and RG.5.45, the first contribution dominates. The energy denominator causes the other 1^+ states to have minimal contribution, resulting in no cancellation in the running sum of the $M1M1$ NME.

V. CONCLUSIONS

First we have studied second-order $M1M1$ transitions for ^{20}Ne, ^{48}Ti, ^{40}Ca and ^{72}Ge with the nuclear shell model. In the case of ^{40}Ca, the full calculation in the valence space is not possible, hence, we tried three different truncations of the valence space. The NME obtained from the second valence space (tr.2) is the most reliable one, given the best description of the 0_2^+ excitation energy. For ^{72}Ge, despite the lack of interactions capable of fully describing second excited states, the NME could be, $\mathcal{M}^{\gamma\gamma}(M1M1) = (0.01 - 0.04)\ \mu_n^2\ \text{MeV}^{-1}$, based on the low-energy spectra, nonetheless we can not disregard larger values, $\mathcal{M}^{\gamma\gamma}(M1M1) = (0.18 - 0.29)\ \mu_n^2\ \text{MeV}^{-1}$.

When comparing the NME obtained for the different nuclei, we find similar values, around $\mathcal{M}^{\gamma\gamma}(M1M1) \simeq 0.1\ \mu_n^2\ \text{MeV}^{-1}$, for ^{20}Ne and for all truncations of ^{40}Ca. For ^{72}Ge the JJ4B and RG.5.45 interactions lead to larger values, $\mathcal{M}^{\gamma\gamma}(M1M1) \simeq 0.25\ \mu_n^2\ \text{MeV}^{-1}$. However, the largest value obtained correspond to the NME of ^{48}Ti, which is approximately three times larger than the value obtained for ^{72}Ge (JJ4B). In the JUN45 and RG.prolate case, we find smaller results compared to all other nuclei, $\mathcal{M}^{\gamma\gamma}(M1M1) \simeq 0.02\ \mu_n^2\ \text{MeV}^{-1}$. In general, we conclude that $M1M1$ NMEs are quite sensitive on the nuclear interaction and the initial and final states of transitions.

Nevertheless, the NMEs discussed in this work have been calculated under the approximation described in Eq.(7), where we assume that the photons share the transition energy. This approximation is valid in the case where $E_n - E_i \gg E_i$, a condition not fulfilled for all the studied nuclei, such as the case of ^{72}Ge. For this reason, it would be interesting for future studies to compare our results with those obtained using Eq.(6) (non-approximated expression). In addition, it would be interesting to calculate energy widths and half-lives, in order to compare the probability of observing these decays with first-order EM transitions and also with future experiments searching for $M1M1$ transitions.

Acknowledgments

First, I would like to express my gratitude to my advisor, Javier Menéndez, for his guidance and support throughout these months. I would also like to give special thanks to Dorian Frycz and Beatriz Romeo for their valuable advice and assistance.

[1] B. Romeo, J. Menéndez, C. Peña Garay. Phys. Lett. B **827**: 136965 (2022).
[2] C. Waltz, H. Scheit, N.Piertralla, T.Aumann, R. Lefol, V. Yu. Ponomarev. Nature **526**:15543 (2015)
[3] M. Goeppert-Mayer. "The shell model". Nobel Lectures, Phys. 1963-1970. http://tinyurl.com/nobel-lectures/mayer-lecture.pdf
[4] A. Poves, F. Nowacki. "The nuclear shell model". Springer:070101 (2001)
[5] J. Suhonen. "From Nucleons to Nucleus. Concepts of Microscopic Nuclear Theory". Springer:003240 (2007)
[6] A. Pérez-Obiol, J. Menéndez, A. Rios, A. M. Romero, A. García-Sáez, B. Juliá-Diaz. Pre-print arxiv. https://arxiv.org/pdf/2302.03641, arxiv:2302.03641v2 (2023)
[7] W. A. Richter, S. Mkhize, B. Alex Brown. Phys. Rev. C **78**:064302 (2008)
[8] Brookhaven National Laboratory. National Nuclear Data Center. https://www.nndc.bnl.gov (2023)
[9] D. G. Frycz. "Nuclear shell model and analytical SU(3) description of ^{28}Si". Final Degree Project. (June 2022)